



HAL
open science

Formation of an Extended Equatorial Shadow Zone for Low-Frequency Saturn Kilometric Radiation

Siyuan Wu, Shengyi Ye, Ulrich Taubenschuss, Georg Fischer, Caitriona M. Jackman, Philippe Zarka, William S. Kurth, Mengmeng Wang, Baptiste Cecconi, Hao Ning, et al.

► **To cite this version:**

Siyuan Wu, Shengyi Ye, Ulrich Taubenschuss, Georg Fischer, Caitriona M. Jackman, et al.. Formation of an Extended Equatorial Shadow Zone for Low-Frequency Saturn Kilometric Radiation. *Geophysical Research Letters*, 2024, 51, 10.1029/2023GL106652 . insu-04853424v2

HAL Id: insu-04853424

<https://insu.hal.science/insu-04853424v2>

Submitted on 23 Dec 2024

HAL is a multi-disciplinary open access archive for the deposit and dissemination of scientific research documents, whether they are published or not. The documents may come from teaching and research institutions in France or abroad, or from public or private research centers.

L'archive ouverte pluridisciplinaire **HAL**, est destinée au dépôt et à la diffusion de documents scientifiques de niveau recherche, publiés ou non, émanant des établissements d'enseignement et de recherche français ou étrangers, des laboratoires publics ou privés.



Distributed under a Creative Commons Attribution 4.0 International License

Geophysical Research Letters®















RESEARCH LETTER

10.1029/2023GL106652

Formation of an Extended Equatorial Shadow Zone for Low-Frequency Saturn Kilometric Radiation

Key Points:

- The propagation characteristics of Saturn Kilometric Radiation (SKR) are established statistically and by ray-tracing
- A shadow region of the low-frequency SKR near the equatorial region at large radial distances is discovered and discussed
- Low-frequency SKR may enter the shadow region due to torus leakage or reflection at the magnetosheath

Siyuan Wu^{1,2} , Shengyi Ye¹ , Ulrich Taubenschuss³ , Georg Fischer⁴ , Caitriona M. Jackman⁵ , Philippe Zarka² , William S. Kurth⁶ , Mengmeng Wang¹ , Baptiste Cecconi² , Hao Ning^{7,8} , Minyi Long⁹ , and Claire Baskevitch² 

¹Department of Earth and Space Sciences, Southern University of Science and Technology, Shenzhen, People's Republic of China, ²LESIA, Observatoire de Paris, Université PSL, CNRS, Sorbonne Université, Université de Paris Meudon, Meudon, France, ³Department of Space Physics, Institute of Atmospheric Physics of the Czech Academy of Sciences, Prague, Czech Republic, ⁴Independent Researcher, Graz, Austria, ⁵School of Cosmic Physics, Dublin Institute for Advanced Studies, Dublin, Ireland, ⁶Department of Physics and Astronomy, University of Iowa, Iowa City, IA, USA, ⁷Institute of Frontier and Interdisciplinary Science, Shandong University, Qingdao, People's Republic of China, ⁸Institute of Space Sciences, Shandong University, Jinan, People's Republic of China, ⁹Department of Space Physics, School of Electronic Information, Wuhan University, Wuhan, People's Republic of China

Supporting Information:

Supporting Information may be found in the online version of this article.

Correspondence to:

S. Ye,
yesy@sustech.edu.cn

Citation:

Wu, S., Ye, S., Taubenschuss, U., Fischer, G., Jackman, C. M., Zarka, P., et al. (2024). Formation of an extended equatorial shadow zone for low-frequency Saturn Kilometric Radiation. *Geophysical Research Letters*, 51, e2023GL106652. <https://doi.org/10.1029/2023GL106652>

Received 13 OCT 2023

Accepted 14 MAY 2024

Abstract Saturn Kilometric Radiation (SKR), being the dominant radio emission at Saturn, has been extensively investigated. The low-frequency extension of SKR is of particular interest due to its strong association with Saturn's magnetospheric dynamics. However, the highly anisotropic beaming of SKR poses challenges for observations. In most cases, the propagation of SKR is assumed to follow straight-line paths. We explore the propagation characteristics of SKR across different frequencies in this study. An extended equatorial shadow region for low-frequency SKR is identified, resulting from the merging of the Enceladus plasma torus and the previously known equatorial shadow zone. Ray-tracing simulations reveal that low-frequency ($\lesssim 100$ kHz) SKR is unable to enter the shadow region and is instead reflected toward high latitudes. In contrast, high-frequency SKR ($\gtrsim 100$ kHz) generally propagates without hindrance. Observations suggest that some low-frequency SKR can enter the shadow region through reflection by the magnetosheath or leakage from the plasma torus.

Plain Language Summary Saturn Kilometric Radiation (SKR) is a natural electromagnetic wave generated in Saturn's high-latitude region along its magnetic field lines. Variations in SKR frequency could offer insights into Saturn's magnetic conditions, especially its interaction with the solar wind. However, the observed frequency characteristics of SKR depend on viewing geometry due to its directional nature. While past studies assumed SKR travels in straight lines, this may not hold true for low-frequency SKR. These emissions can change direction when they encounter dense plasma, similar to light reflecting off a mirror or bending when entering water. At Saturn's equatorial region, the plasma torus created by Enceladus, one of Saturn's moons, contains dense plasma and significantly affects radio wave propagation. Our study investigates the distribution of SKR at different frequencies and identifies a shadow region where low-frequency SKR emissions are rarely seen. Using numerical simulations of ray propagation paths, we discover that low-frequency SKR emissions cannot reach these shadow regions because they are reflected by the dense plasma torus. However, occasionally, we observe low-frequency SKR in the shadow region, suggesting the possibility of reflection by Saturn's magnetosheath or leakage through the plasma torus.

1. Introduction

Saturn's Kilometric Radiation (SKR) was first detected during the Voyager Saturn approach in the 1980s (Kaiser et al., 1980) and was extensively investigated by the subsequent Cassini mission (Cecconi et al., 2009; Fischer et al., 2009; Lamy, Zarka, Cecconi, Hess, & Prangé, 2008; Lamy, Zarka, Cecconi, Prangé, et al., 2008; Lamy et al., 2009, 2011, 2013, 2018; Taubenschuss et al., 2021; Wu et al., 2022a) as summarized by Lamy (2017). Saturn Kilometric Radiation spans a frequency range from a few kilohertz (kHz) to one megahertz (MHz) and primarily manifests as Right-Hand Extraordinary (R-X) mode, occasionally accompanied by weaker Left-Hand Ordinary (L-O) mode emission (Lamy, Zarka, Cecconi, Prangé, et al., 2008). The source region of SKR displays shell electron distributions, and the generation mechanism is attributed to the cyclotron maser instability along

auroral field lines above Saturn's polar regions (Kurth et al., 2011; Lamy et al., 2018; Wu & Lee, 1979; Zarka, 1998).

The CMI-generated emissions beam at large angles along a thin hollow cone whose axis is aligned with the local magnetic field in the source (Hess et al., 2008; Mutel et al., 2010). This beaming pattern is responsible for a highly anisotropic emission with strong visibility effects, so the observed SKR time-frequency features strongly depend on the observer's location (Cecconi et al., 2009; Lamy, Zarka, Cecconi, Hess, & Prangé, 2008, Lamy et al., 2013). While theory favors perpendicular propagation inside the source region due to shell electron distributions (Lamy et al., 2011), the apparent beaming angles of SKR observed at some distance to the source are smaller than predicted (Cecconi et al., 2009; Lamy, Zarka, Cecconi, Prangé, et al., 2008; Lamy et al., 2018), implying refractions and reflections during the outward propagation from the source region. The highly oblique SKR beaming leads to an equatorial shadow zone (ESZ) formed at small radial distances (Cecconi et al., 2009; Lamy, Zarka, Cecconi, Hess, & Prangé, 2008; Lamy et al., 2010). The ESZ extends around 5 Saturn Radii (R_s) at the equator, with its shape varying with emission frequencies (Lamy, Zarka, Cecconi, Hess, & Prangé, 2008). Enceladus plasma torus (EPT), formed by the cryovolcanic activity of Saturn's icy moon Enceladus, and centered at 4 R_s at the equator (Persoon et al., 2020), may cause significant refraction of the low-frequency SKR ($\lesssim 100$ kHz), while high-frequency SKR ($\gtrsim 100$ kHz) propagates through it (Lamy et al., 2010). However, no dedicated propagation study has been carried out so far.

The low-frequency extensions (LFE) of SKR serve as an important indicator for reconnection events and compression-induced hot plasma injections at Saturn (Bunce et al., 2005; Cecconi et al., 2022; Jackman et al., 2009, 2010, 2023; Reed et al., 2018). Understanding their propagation is crucial for uncovering their further magnetospheric implications. Some low-frequency SKR exhibit unique time-frequency morphologies and are identified as “caterpillar” emissions (Fischer et al., 2022; Fischer et al., 2023; O'Dwyer et al., 2023). These emissions, typically observed near 10 kHz, often display depolarization features (low polarization degree of the Stokes parameters) whose generation mechanisms remain unknown but may involve refractions and reflections during propagation. This study examines SKR propagation, particularly its low-frequency emissions by both data-based statistics and ray-tracing simulations.

2. Data and Methodology

2.1. Cassini Data

The wave data were collected by the Cassini Radio and Plasma Wave Science (RPWS) High Frequency Receiver (Gurnett et al., 2004). The circular polarization parameters were obtained using the approach outlined by Cecconi and Zarka (2005). The electron cyclotron frequency f_{ce} (proportional to the local magnetic field amplitude B) and the electron plasma frequency f_{pe} (proportional to the square root of the electron density n_e) were computed based on magnetic field data from Cassini's magnetometer (Dougherty et al., 2004) and electron moments data from the CAPS instrument (Young et al., 2004).

We conducted a comprehensive analysis of the SKR distribution across various frequencies by applying a data cleaning process to the Cassini RPWS spectrograms covering the period from 2004 DOY (day of year) 001 to 2017 DOY 258. The selected frequency range encompasses the full SKR frequency spectrum, spanning from 3.68 kHz to 1 MHz. For the high-frequency part ($\gtrsim 100$ kHz), the spectrograms predominantly contained SKR emissions, simplifying the processing. Other emissions likely occur in the high-frequency range of SKR include Solar type III bursts, often unpolarized, and sporadic Saturn Electrostatic Discharges, occasionally reaching down to 800 kHz. In the lower frequency range, SKR emissions often coexisted with other signals, including L-O mode 5 and 20 kHz Saturn Narrowband (NB) emissions (Wu et al., 2021; Ye et al., 2009), L-O mode Saturn Anomalous Myriametric (SAM) radiation (Wu et al., 2022c) and sporadic electrostatic emissions like electron cyclotron harmonics (ECH, Long et al., 2021). To isolate SKR signals, we utilized event lists provided by Wu et al. (2021, 2022b) to remove NB and SAM emissions. Additionally, we filtered out ECH by discarding spectrogram pixels exceeding the local f_{ce} up to $7/2 f_{ce}$ values, as recommended by Long et al. (2021).

The processed SKR spectra were subjected to a 2D median filter using a (3 channels * 3 channels) kernel (across time and frequency) to remove isolated pixels. We also excluded emissions that were weak (< 20 dB, with a background level of $10^{-17} \text{ V}^2 \text{ Hz}^{-1}$) and unpolarized ($|V| \leq 0.3$, with V the Stokes parameter for circular polarization). The later criterion typically eliminates sporadic Solar type III bursts. Notably, certain non-SKR

emissions, including R-X mode harmonics of NB emissions (Ye et al., 2011), residual NB emissions, and specific electrostatic noise, were present in the data but challenging to remove entirely. However, their impact on our results is minimal due to their lower occurrence compared to SKR. To further mitigate their influence, the final statistical analysis concentrated on the frequency range above 6 kHz. Additionally, data from 2017 was excluded due to substantial electrostatic noise in the low-frequency range.

2.2. ARTEMIS-P Simulations

The ray-tracing method utilized here is the ARTEMIS-P algorithm (Anisotropic Ray Tracer for Electromagnetics in Magnetosphere, Ionosphere, and Solar Wind, including Polarization; Gautier, 2013; Gautier et al., 2013), as used in Wu et al. (2024). Calculations incorporate Saturn's magnetic field model (Dougherty et al., 2018) and EPT model (Persoon et al., 2006). SKR rays are launched at frequencies [1,000, 500, 200, 100, 80, 60, 40, 30, 20, 10, 6] kHz along L-shell = 15 (corresponding to invariant latitude 75°, roughly the SKR source latitude; Cecconi et al., 2009; Lamy et al., 2009), at positions having local f_{ce} values of [990, 490, 190, 95, 75, 55, 35, 28, 19, 9, 5] kHz. Launching the rays with wave frequencies close to and slightly higher than the local f_{ce} in the determined source positions is due to the technical limitation of the ray-tracing algorithm, which adheres to the cold plasma dispersion relation and precludes initiation of R-X mode rays at positions with wave frequencies equal to or below the local f_{ce} values (Lamy et al., 2010, 2018). Therefore, the rays are launched at positions with the wave frequencies close to and slightly higher than the local f_{ce} values, as also adapted in the previous studies (Hashimoto et al., 1998a; Hashimoto et al., 1998b; Ladreiter & Leblanc, 1990). The initial beaming angle of SKR is set to be 90° according to the previous studies (Lamy et al., 2011, 2018).

3. Observations of SKR Near the Enceladus Plasma Torus and Magnetosheath

Figure 1 presents SKR observations potentially indicating refractions and reflections near the EPT and magnetosheath. The R-X mode SKR displays a low-frequency cutoff at the frequency $f_{RX} = \frac{1}{2}f_{ce} + \sqrt{f_{pe}^2 + \frac{f_{ce}^2}{4}}$. Elevated plasma densities at the EPT boundary lead to a sufficiently high f_{RX} for SKR reflection. Panels (a)–(b) of Figure 1 reveal variations in the low-frequency limits of SKR, consistent with Cassini's proximity to the EPT. These low-frequency SKR emissions might be reflected in other directions at the EPT boundary, thereby evading Cassini's detection. The intricate circular polarization pattern in panel (b) within the equatorial region results from the superposition of SKR emissions originating from both hemispheres, which exhibit right-hand circular polarization (~ -1 , in red) at the northern hemisphere and exhibit left-hand circular polarization in the southern hemisphere (~ 1 , in blue).

The second case in panel (c)–(d) provides a clearer demonstration of SKR cutoff at the EPT. The intensified “line” emissions correspond to local upper hybrid waves at f_{uh} (upper hybrid frequency, $f_{uh} = \sqrt{f_{pe}^2 + f_{ce}^2}$). Notably, the f_{RX} frequency at the EPT boundary closely aligns with the local f_{uh} , resulting in a distinct cutoff pattern of SKR along this “line.” These cutoff emissions exhibit reduced intensity, while higher-frequency emissions experience minor attenuation upon entering the EPT. Additionally, panel (d) reveals depolarization characteristics of these cutoff emissions (Stokes V ~ 0 , the linear and total polarization degree (not shown) are also lower). The partial absence of SKR around the center of panel (c) is likely to be due to the ESZ as Cassini gets as close as ~ 4 Rs.

Panels (e)–(f) reveal distinctive cutoff patterns as the spacecraft traverses the EPT and progresses outward to larger radial distances in the equatorial region. The EPT obstructs SKR below approximately 100 kHz. Notably, a sudden occurrence of the emission below 100 kHz at 08-04 10:00 UT in panel (e) is evident, suggesting potential “leakage” from the EPT or distant reflection (magnetosheath reflection) of these low-frequency emissions. At that time Cassini was positioned 25 Rs from Saturn, near the dayside magnetopause at noon local time. The “leaked” or reflected low-frequency SKR displays attenuation and depolarization similar to that seen in panel (c), possibly due to refractions and reflections caused by the EPT or magnetosheath.

Panels (g)–(h) exhibit a clear cutoff pattern of the low-frequency SKR below ~ 10 kHz within the magnetosheath, implying its potential for reflecting such frequencies, akin to the reflection observed in the 5 kHz NB emissions (Wu et al., 2022b). The pink line represents the local f_{pe} , which is nearly identical to the local f_{RX} within the magnetosheath due to the weak magnetic field. Note that the emission around 10 kHz in Figure 1 panel (e) at

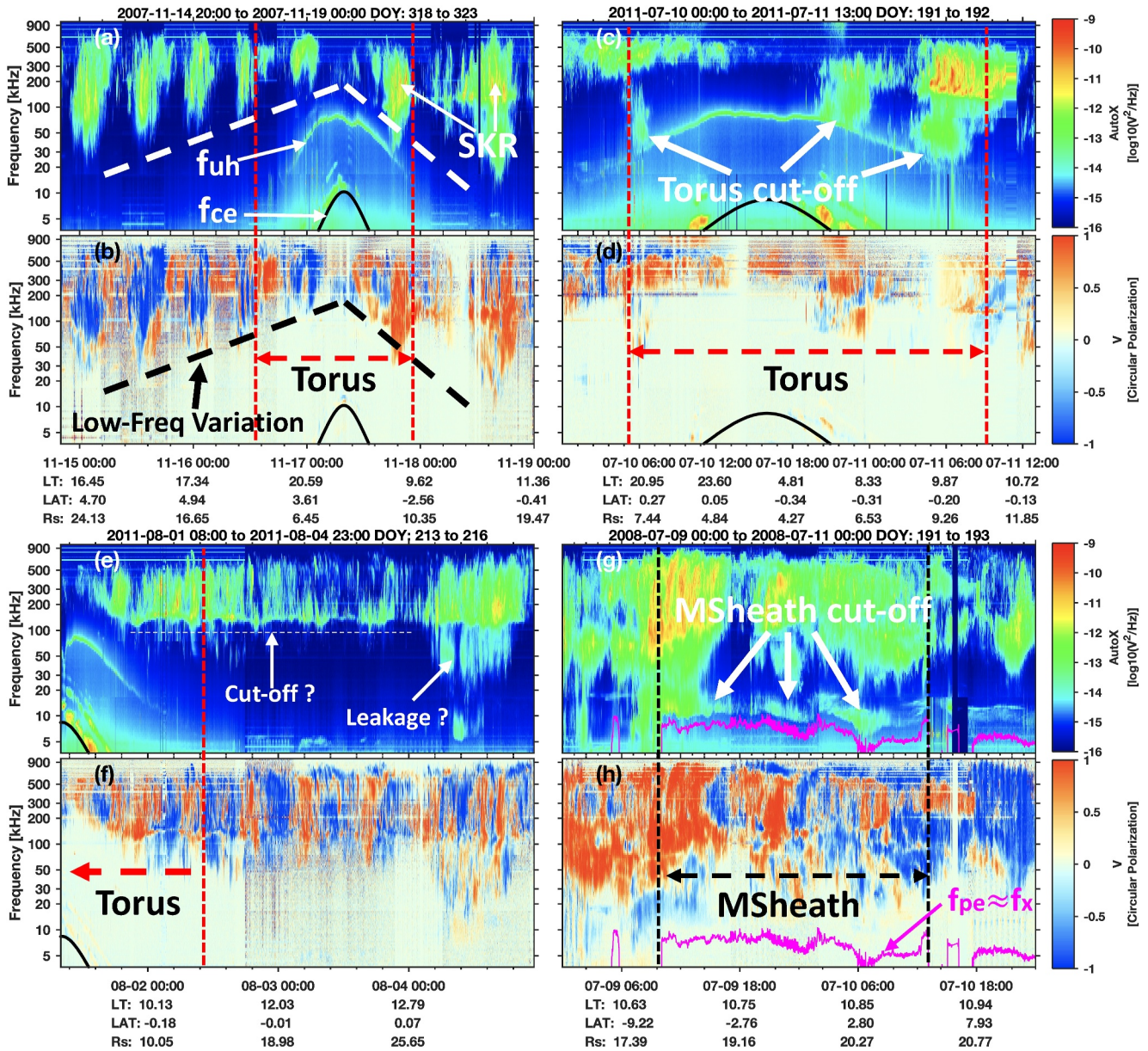


Figure 1. Observations of Saturn Kilometric Radiation near the Enceladus plasma torus (EPT) and within the magnetosheath. Panel (a) shows the wave electric field spectrogram. Panel (b) displays the circular polarization. Vertical red lines indicate the approximate location of the EPT. The white and black dashed lines highlight low-frequency variations. Panels (c)–(h) present three additional observations in the same format as panels (a)–(b). The black vertical lines in panels (g)–(h) delineate the magnetosheath, and the pink line represents the local f_{pe} frequency in the magnetosheath, which roughly equals the local f_x frequency due to the weak magnetic field (see text).

10:00 SCET on 08-04 2011 and the enduring emission in Figure 1 panel (g) just above the magnetosheath cutoff are recognized as caterpillar emissions.

4. Statistical Distribution of SKR at Different Frequencies

Figure 1 displays observations suggesting potential refractions and reflections of low-frequency SKR near the EPT. To explore SKR propagation at various frequencies, we present statistical occurrence rates in Figure 2, segmented into frequency bands. High-frequency SKR (panels (a)–(c), ≥ 100 kHz) can propagate across the region near Saturn, forming a small ESZ denoted by the triangular area between two pink lines, with lower

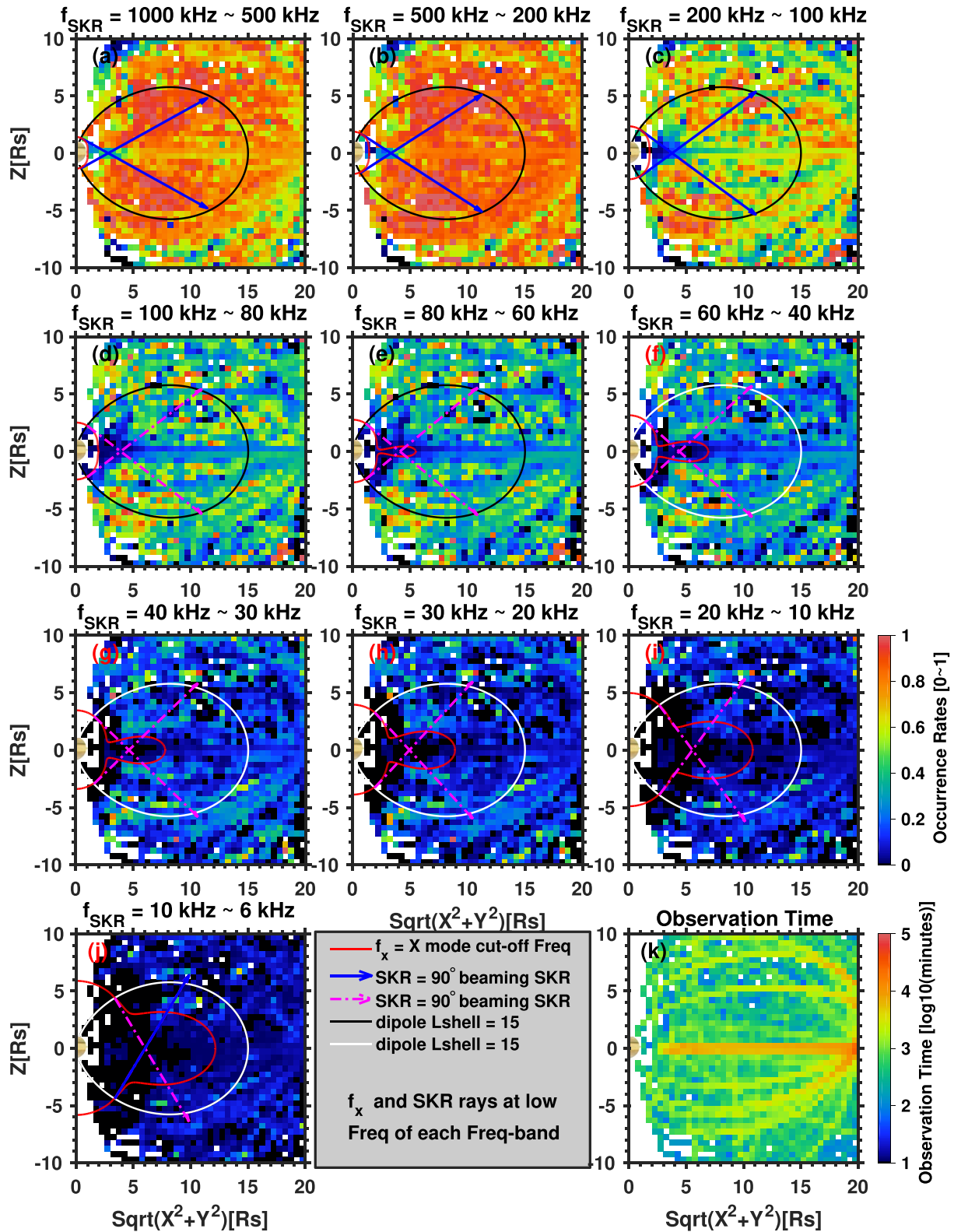


Figure 2.

occurrence rates at the equator (Lamy, Zarka, Cecconi, Hess, & Prangé, 2008). Additionally, high-frequency SKR exhibits higher occurrence rates compared to low-frequency SKR.

In panels (a)–(d), the ESZ region expands radially, as indicated by the dark blue area. For SKR frequencies above ~ 80 kHz, the f_{RX} contour lines (red lines in panels (a)–(d)) lie within the ESZ region. However, in panel (e), the f_{RX} contours at ~ 60 kHz suddenly protrude, forming a boundary around the inner part of the EPT due to the higher plasma density there. The R-X mode SKR cannot propagate in regions where the wave frequency is less than f_{RX} . Consequently, the shadow region becomes a combination of the triangular ESZ shape and a torus-shaped region for the low-frequency SKR below ~ 60 kHz. For convenience, we refer to these f_{RX} encircled regions as the R-X mode Forbidden Zone (FZ). As the SKR wave frequency decreases and as depicted in panels (e) to (j), the FZ region expands. The lower occurrence rates within this FZ region indicate that low-frequency SKR cannot propagate into these areas and are likely reflected to other directions. Note that the merging of ESZ and the torus-shaped FZ region appears to start within the 80–100 kHz frequency range and not the 60 kHz, as depicted in panel (d), which we attribute to the uncertainties in the EPT density model and magnetic field model. There are still some emissions observed inside the ESZ and FZ, for example, light blue patches inside the red contour in panel (i), these are due to the uneliminate NB emissions and ECH waves at the lower frequencies.

5. Merging of the Equatorial Shadow Zone and the R-X Mode Forbidden Zone

The low-frequency SKR distributions in Figure 2 exhibit regions of low occurrence rates, indicating an extension of the shadow region that is further explored in Figure 3, panels (a)–(b). This analysis employs the magnetic field model by Dougherty et al. (2018) and the EPT electron density model by Persoon et al. (2006). Panel (a) depicts the theoretical beaming pattern of SKR in both hemispheres, with a fixed beaming angle of 90° and no refraction effects. The ESZ forms at the equator and expands away from Saturn as SKR frequencies decrease, which covers a radial distance within 6 Rs. In panel (b), the contour lines of f_{RX} illustrate the shape of the R-X mode FZ. The f_{RX} at the EPT is at approximately $f_{RX} = 60$ kHz as derived from the analytical models, but may be as high as 100 kHz as suggested by the observation in Figure 2 panel (d). The FZ extends to ~ 12 Rs when f_{RX} is 6 kHz. The actual shadow region for SKR at a specific frequency combines the corresponding areas shown in panels (a) (ESZ) and (b) (FZ) of Figure 3. At higher frequencies, the shadow region primarily aligns with the ESZ since f_{RX} contours fall within it. Conversely, at lower frequencies ($f_{SKR} \lesssim 100$ kHz), the ESZ expands and merges with the region defined by the f_{RX} contours, eventually becoming enclosed by the FZ. Consequently, low-frequency SKR encounters reflections at the FZ boundary, explaining the absence of low-frequency SKR within the FZ region in Figure 1. Moreover, this implies the potential existence of an extended shadow zone beyond the FZ or the EPT at larger radial distance due to the blocking effect.

For a clearer SKR propagation illustration, we conducted ray-tracing calculations using Saturn's plasma environment as shown in Figure 3 panel (c). Rays of varying frequencies were launched from the designated sources. The EPT electron density is color-coded in the background. Panel (c) illustrates that high-frequency SKR can freely traverse the dense EPT. Conversely, frequencies below approximately 100 kHz lead to pronounced refraction (rays being bent, e.g., rays at 100 kHz) and reflection (rays being reflected to other directions, e.g., rays at 20 kHz) by the EPT, causing rays to bend toward higher latitudes. This creates an extended shadow zone from ESZ + FZ to beyond the EPT, outlined by the shaded box in panel (c). We then refer to the extended ESZ as extended equatorial shadow zone (EESZ), which roughly covers a radial distance from ~ 12 Rs and beyond. However, the EESZ beyond the EPT is not observed in the actual distribution in Figure 2. Surprisingly, low-frequency emissions are detected in this area, especially at larger radial distances as shown in Figure 2. This raises questions about the propagation of SKR and how it manages to reach these regions. For high-frequency SKR, the absence of blockage by the FZ allows the waves to traverse the EPT, the emissions observed in the EESZ can be simply explained by the movement of source field lines, altering the initial beaming angle of SKR, or simply due to the 3D hollow cone beaming of SKR, thus parts of it are beamed out of the meridian plane into the EESZ. Indeed, various direction-finding studies show that

Figure 2. Statistical distribution of Saturn Kilometric Radiation (SKR) in the meridian plane separated in different frequency bands. Panel (a) displays the occurrence rates distribution of SKR ranging from 1,000 to 500 kHz. Pink and blue arrows indicate two SKR rays with beaming angles of 90° and wave frequencies of 500 kHz, originating from the $L = 15$ magnetic field line (black solid line). The red contour line near the planet represents the R-X mode cutoff frequency: $f_{RX} = 500$ kHz, derived using the Enceladus plasma torus model (Persoon et al., 2006) and magnetic field model (Dougherty et al., 2018). Panels (c)–(j) illustrate the distribution of SKR at the other frequency bands. Panel (k) shows the corresponding Cassini observation time.

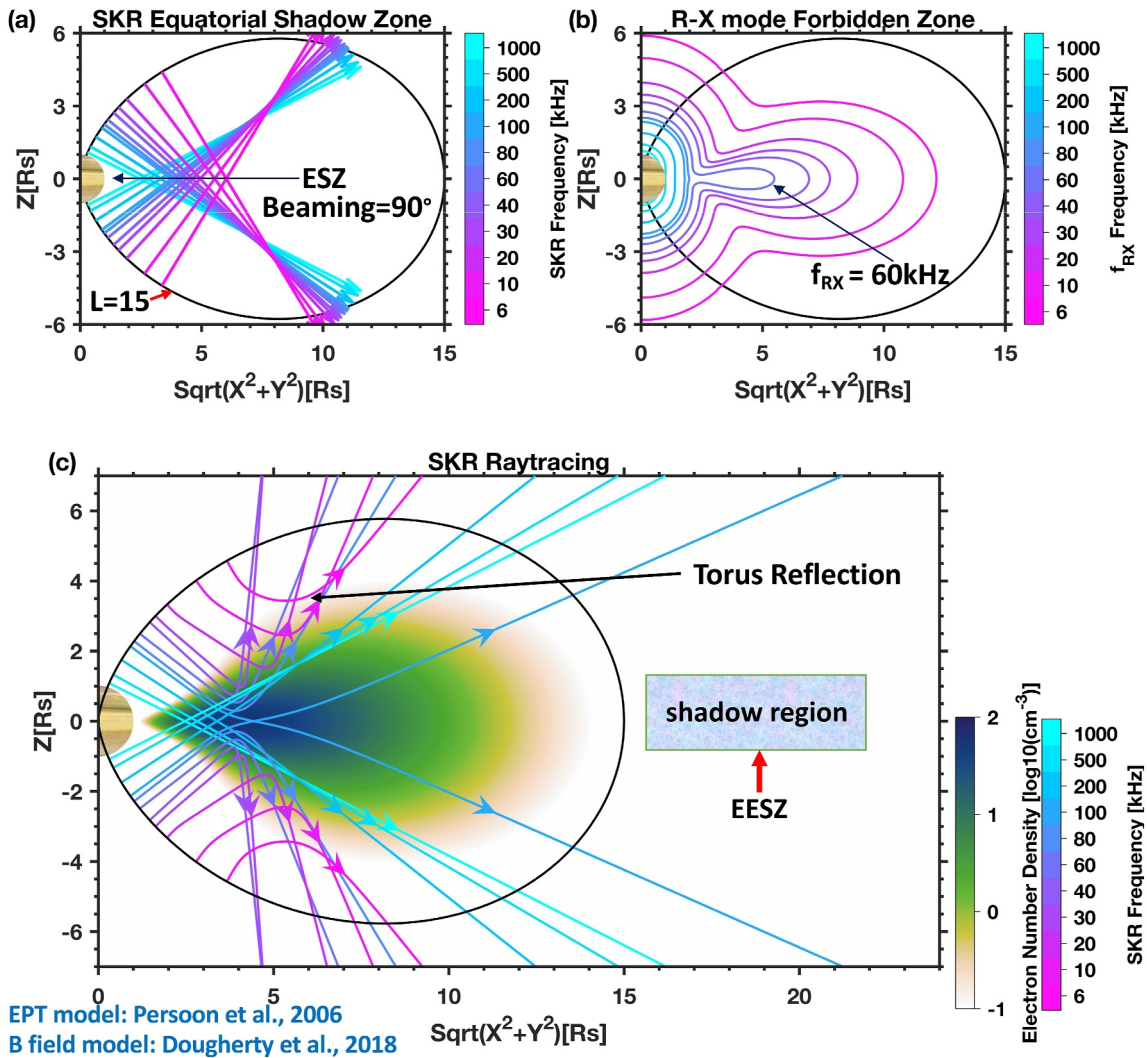


Figure 3. Merging of the equatorial shadow zone and R-X mode Forbidden Zone (FZ). Panel (a) displays the beaming pattern of Saturn Kilometric Radiation (SKR) at various frequencies without refraction effects. The beaming angle is chosen to be 90°. The source locations are along the $L = 15$ magnetic field line. Panel (b) illustrates the contours of f_{RX} at different frequencies, calculated using the Dougherty et al. (2018) magnetic field model and Persoon et al. (2006) Enceladus plasma torus model. These f_{RX} contours define the boundaries of the FZ. Panel (c) presents the ray-tracing calculation of SKR propagation with the electron density presented by the background color-code.

the SKR sources are not located at the central meridian where the spacecraft resides, but rather on the east and west side of the planet, with respect to the position of the observer (e.g., Cecconi et al., 2009; Lamy et al., 2009, 2013). However, for low-frequency SKR, these emissions would be expected to be reflected at the FZ boundary, with no rays able to penetrate the dense EPT regardless of the movement of source field lines and the 3D geometry of their beaming pattern. Note that the possible refraction of the rays near the source region is not considered in the simulations, which may lead the initial beaming angle of the rays to be smaller than 90°. This scenario is also tested in the ray-tracing calculations (see Figure S1), which give consistent pattern with the results presented here. The size of EESZ will shrink if we consider smaller beaming angles.

6. Reflection by Magnetosheath and Leakage Through the EPT

Figure 4 panel (a) provides a clearer illustration of the low-frequency emissions observed in the EESZ based on 2011 RPWS data. Cassini's orbits during 2011 were primarily within the equatorial latitude range of -0.83° – 0.38° . The measured wave electric field was stacked and averaged to create a frequency versus radial distance spectrum, representing observations within the EESZ. Panel (a) reveals that emissions below 100 kHz are

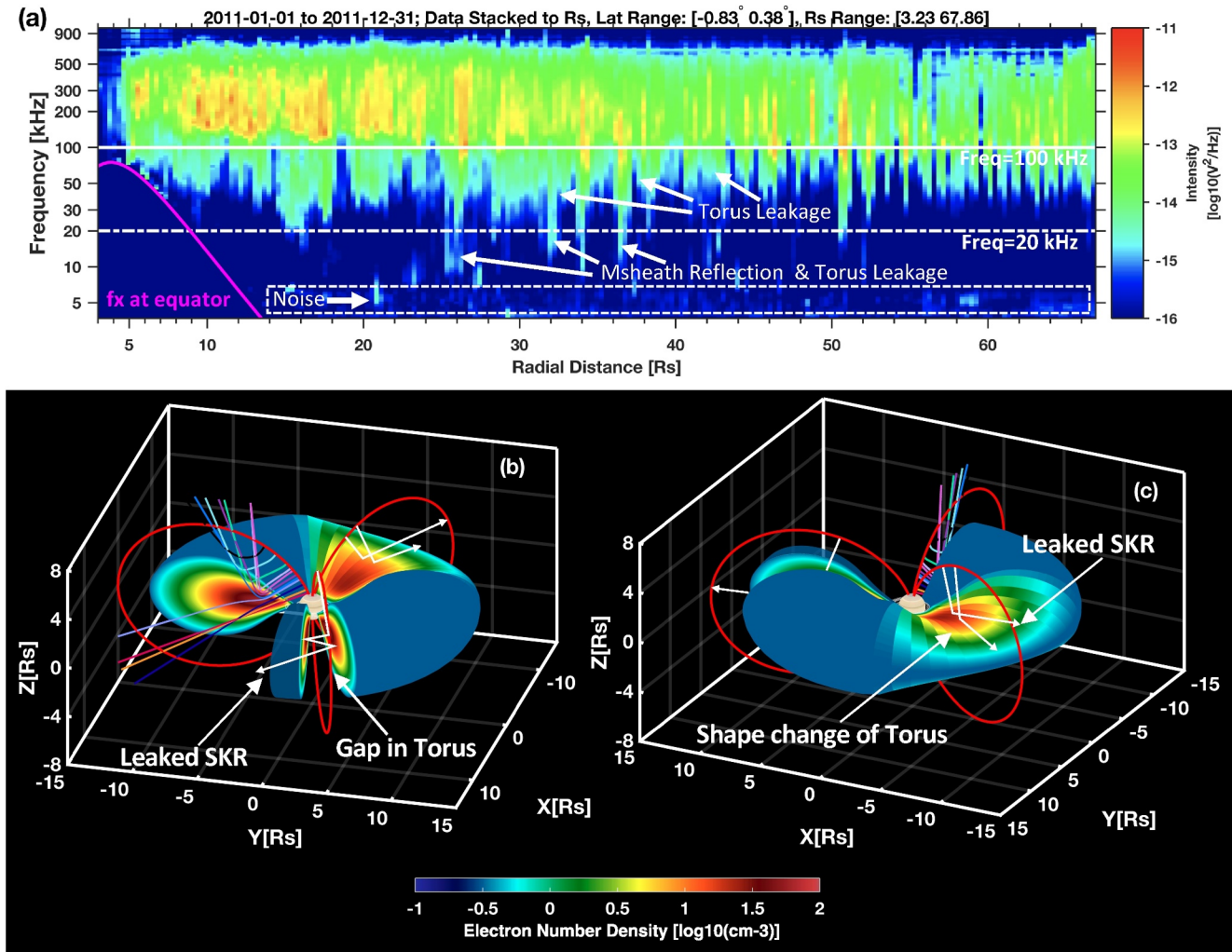


Figure 4. Reflected and leaked low-frequency Saturn Kilometric Radiation (SKR) emissions. Panel (a) displays the stacked wave spectrogram measured near the equator during 2011. The pink line represents the f_{RX} frequency as a function of radial distance, calculated using the modeled magnetic field and plasma density along the equatorial radial direction. Low-frequency emissions below 10 kHz are labeled as noise due to NB emissions or electrostatic noise that couldn't be fully eliminated. Panel (b) illustrates a possible gap within the Enceladus plasma torus (EPT), while panel (c) depicts a shape change in the EPT. The colored lines correspond to the rays shown in Figure 3 panel (c). The red lines represent three L-shells at $L = 15$. The white arrow lines are manually drawn to indicate possible ray paths of the leaked SKR.

frequently observed, with some extending to frequencies below 20 kHz, indicating a “filling” of the EESZ by low-frequency SKR. This filling phenomenon is reminiscent of the 5 kHz Saturn NB emissions, where L-O mode NB emissions are reflected by the EPT toward high latitudes, creating an ESZ that is later filled by reflected emissions from the magnetosheath (Wu et al., 2021, 2022b).

We propose that the magnetosheath of Saturn may also be capable of reflecting low-frequency SKR, the reflected emissions will propagate toward the EESZ, which potentially explains their presence in the EESZ. When the magneosheath-reflected rays propagate toward the EPT, they could be reflected at the EPT boundary again. However, based on statistical studies of the magnetosheath electron density at Saturn (Sergis et al., 2013), the maximum frequency of waves reflected by the magnetosheath should be less than a certain frequency threshold: assume the maximum magnetosheath electron density to be 2 cm^{-3} and the magnetic field to be 5 nT (Sergis et al., 2013), the calculated $f_{RX} \approx 12.7 \text{ kHz}$. The statistical distribution of the 20 kHz Saturn NB emissions suggests that the 20 kHz L-O mode emissions are rarely reflected by the magnetosheath. Therefore, magnetosheath reflection may only account for SKR emissions observed in the EESZ below $\sim 20 \text{ kHz}$ (or even below 12.7 kHz). Panel (a) also indicates that emissions below 20 kHz, that is, the possible sheath-reflected emissions, are not observed at small radial distance close to the EPT.

Emissions observed in the EESZ with frequencies above 20 kHz may be leaked from the EPT. The leaked emissions are observed near or even inside the EPT, for example, at 10 Rs as shown by Figure 4 panel (a) and as visible by the SKR lower-frequency cutoff in Figure 1 panels (c)–(d). Note that the emissions below 20 kHz may also leak from the EPT. The leakage of low-frequency SKR from the EPT can occur due to spatial changes, such as density gaps, shape variations, or density asymmetries (Holmberg et al., 2014; Schippers et al., 2013), as well as temporal changes, like periodic variations of the EPT (Khurana et al., 2009). These factors enable the passage of low-frequency SKR, leading them to eventually reach the EESZ, as depicted in Figure 4 panels (b)–(c). The propagation of low-frequency SKR through the EPT may involve multiple reflections and refractions as depicted in panel (b), which can result in attenuation and depolarization of the emissions, as observed in Figure 1 panels (c)–(d). Note that it seems that the most “smoothed” torus-leaked emissions are observed within 40 Rs as shown in panel (a).

7. Discussion and Summary

The impact of radio emission propagation by the “plasma torus” or the “plasma disk” at Jupiter has been previously documented (Boudjada et al., 2001; Desch et al., 1994; Gurnett et al., 1998; Higgins et al., 1999; Kaiser et al., 1996; Louarn et al., 1998, 2000, 2001), which underscore the significance of activities and structures within the Io plasma torus. At Saturn, not many investigations focus on the dynamics of the EPT, but rather delve into the activities of the Enceladus plume (neutrals and water ions), encompassing variations across different timescales (Hansen et al., 2017; Ingersoll & Ewald, 2017). The longitudinal modulation of the inner plasma disk (Gurnett et al., 2007), dayside/nightside asymmetry (Holmberg et al., 2014; Schippers et al., 2013), flapping of the plasma disk (Khurana et al., 2009), and plasma evacuation events (Louarn et al., 2007) have also been observed. Consequently, the actual propagation characteristics of the SKR may exhibit more complexity than discussed in this study. It's also important to consider refraction near the radio source region alongside torus dynamics as suggested by beaming angle studies (Cecconi et al., 2009; Lamy, Zarka, Cecconi, Hess, & Prangé, 2008). While no clear electron cavity is observed in the SKR source region, emissions could still be refracted when the wave frequency approaches the f_{RX} frequency (Lamy et al., 2018). Similar ray-tracing calculations (Figure S1) considering this effect yielded consistent results as presented here.

The EPT plays a crucial role in impeding radio wave propagation at Saturn, creating challenges for low-frequency radio emission observations (Wu et al., 2022b; Ye et al., 2010). In the equatorial region outside the EPT, the merging of the ESZ and FZ results in the formation of an extended shadow region for low-frequency SKR. This discovery provides an initial understanding of the favorable observation geometry for low-frequency SKR, especially for LFE events that are usually used as indicators of magnetospheric dynamics (Jackman et al., 2009). The “filling” of the shadow region suggests the involvement of magnetosheath reflection and EPT leakage, presenting an opportunity to investigate the dynamics of the magnetosheath and EPT using low-frequency SKR observations in the shadow region. Moreover, this work offers plausible explanations for the propagation characteristics of the recently reported caterpillar emissions (Fischer et al., 2023; Fischer et al., 2022). The smooth time-frequency features and depolarization exhibited by the caterpillar emissions can be qualitatively attributed to multiple reflections within the EPT or the magnetosheath.

Data Availability Statement

The Cassini MAG data and CAPS data were downloaded from the Planetary Data System at (MAG: Dougherty et al., 2019; CAPS: Waite & Furmanm, 2013). The Cassini RPWS data used in this work were downloaded from the LESIA/Kronos collection with $n2$ level data (Cecconi et al., 2017a) and $n3d$ data (Cecconi et al., 2017b; goniopolarimetric data obtained using the method Cecconi & Zarka, 2005). The Artemis- P source code can be found at Gautier, Baskevitch and Cecconi. (2023).

References

- Boudjada, M. Y., Galoapeau, P. H. M., & Rucker, H. O. (2001). Jovian hectometric beam observed by PWS and WAVES experiments on board Galileo and Wind spacecraft. *Planetary and Space Science*, 49(10), 1151–1158. [https://doi.org/10.1016/S0032-0633\(01\)00022-8](https://doi.org/10.1016/S0032-0633(01)00022-8)
- Bunce, E. J., Cowley, S. W. H., Wright, D. M., Coates, A. J., Dougherty, M. K., Krupp, N., et al. (2005). In situ observations of a solar wind compression-induced hot plasma injection in Saturn's tail. *Geophysical Research Letters*, 32(20), L20S04. <https://doi.org/10.1029/2005GL022888>
- Cecconi, B., Lamy, L., & Zarka, P. (2017a). Cassini/RPWS/HFR LESIA/Kronos N2 data collection (Version 1.0) [Dataset]. *PADC*. <https://doi.org/10.25935/XS9J-ND90>

Acknowledgments

This work was supported by the Strategic Priority Research Program of the Chinese Academy of Sciences (Grants XDB 41000000). SY and SW thank the support of NSF projects 42274221 and 42074180. We thank the support of Science, Technology and Innovation Commission of Shenzhen Municipality program (STIC20200925153725002). SY and SW thank the support of the Guangdong province program (Grants 2021CX02Z468). UT and GF acknowledge support from the FWF-GACR international project I4559-N/20-06802L.

- Cecconi, B., Lamy, L., & Zarka, P. (2017b). Cassini/RPWS/HFR LESIA/Kronos N3e Data Collection (Version 1.0) [Dataset]. *PADC*. <https://doi.org/10.25935/9ZAB-FP47>
- Cecconi, B., Lamy, L., Zarka, P., Prangé, R., Kurth, W. S., & Louarn, P. (2009). Goniopolarimetric study of the revolution 29 Perikrone using the Cassini Radio and Plasma Wave Science instrument high-frequency radio receiver. *Journal of Geophysical Research*, *114*(3), 1–19. <https://doi.org/10.1029/2008JA013830>
- Cecconi, B., Witasse, O., Jackman, C. M., Sánchez-Cano, B., & Mays, M. L. (2022). Effect of an interplanetary coronal mass ejection on Saturn's radio emission. *Frontiers in Astronomy and Space Sciences*, *9*, 800279. <https://doi.org/10.3389/fspas.2022.800279>
- Cecconi, B., & Zarka, P. (2005). Direction finding and antenna calibration through analytical inversion of radio measurements performed using a system of two or three electric dipole antennas on a three-axis stabilized spacecraft. *Radio Science*, *40*(3), 1–20. <https://doi.org/10.1029/2004RS003070>
- Desch, M. D., Farrell, W. M., & Kaiser, M. L. (1994). Asymmetries in the Io plasma torus. *Journal of Geophysical Research*, *99*(A9), 17205–17210. <https://doi.org/10.1029/94JA01615>
- Dougherty, M. K., Cao, H., Khurana, K. K., Hunt, G. J., Provan, G., Kellock, S., et al. (2018). Saturn's magnetic field revealed by the Cassini Grand Finale. *Science*, *362*(6410), eaat5434. <https://doi.org/10.1126/science.aat5434>
- Dougherty, M. K., Kellock, S., Slootweg, A. P., Achilleos, N., Joy, S. P., & Mafi, J. N. (2019). *Cassini orbiter MAG calibrated summary averaged V2.1, CO-E/SW/IS-MAG-4-SUMM-1MINAVG-V2.1*. NASA Planetary Data System. <https://doi.org/10.17189/5rhj-sm88>
- Dougherty, M. K., Kellock, S., Southwood, D. J., Balogh, A., Smith, E. J., Tsurutani, B. T., et al. (2004). The Cassini magnetic field investigation. *Space Science Reviews*, *114*(1), 331–383. <https://doi.org/10.1007/s11214-004-1432-2>
- Fischer, G., Cecconi, B., Lamy, L., Ye, S.-Y., Taubenschuss, U., Macher, W., et al. (2009). Elliptical polarization of Saturn Kilometric Radiation observed from high latitudes. *Journal of Geophysical Research*, *114*(A8), A08216. <https://doi.org/10.1029/2009JA014176>
- Fischer, G., Taubenschuss, U., & Pisa, D. (2022). Classification of spectral fine structures of Saturn Kilometric Radiation. *Annals of Geophysics*, *40*(4), 485–501. <https://doi.org/10.5194/angeo-40-485-2022>
- Fischer, G., Taubenschuss, U., Pisa, D., Lamy, L., Wu, S.-Y., Ye, S.-Y., et al. (2023). A particular form of Saturn Kilometric Radiation at the low end of its spectrum. In C. K. Louis, C. M. Jackman, G. Fischer, A. H. Sulaiman, & P. Zucca (Eds.), *Planetary radio emissions IX*. published by Trinity College Dublin. <https://doi.org/10.25546/103099>
- Gautier, A.-L. (2013). *Étude de la propagation des ondes radio dans les environnements planétaires (Doctoral dissertation)*. Observatoire de Paris.
- Gautier, A. L., Baskevitch, C. A., & Cecconi, B. (2023). Maserlib/ARTEMIS-P: Version 0.1.0 (v0.1.0). *Zenodo*. <https://doi.org/10.5281/zenodo.8055943>
- Gautier, A.-L., Cecconi, B., & Zarka, P. (2013). ARTEMIS-P: A general Ray Tracing code in anisotropic plasma for radioastronomical applications. In *Proceedings of the 2013 international symposium on electromagnetic theory* (pp. 1–4).
- Gurnett, D. A., Kurth, W. S., Kirchner, D. L., Hospodarsky, G. B., Averkamp, T. F., Zarka, P., et al. (2004). The Cassini radio and plasma wave investigation. *Space Science Reviews*, *114*(1), 395–463. <https://doi.org/10.1007/s11214-004-1434-0>
- Gurnett, D. A., Kurth, W. S., Menietti, J. D., & Persoon, A. M. (1998). An unusual rotationally modulated attenuation band in the Jovian hectometric radio emission spectrum. *Geophysical Research Letters*, *25*(11), 1841–1844. <https://doi.org/10.1029/98GL01400>
- Gurnett, D. A., Persoon, A. M., Kurth, W. S., Groene, J. B., Averkamp, T. F., Dougherty, M. K., & Southwood, D. J. (2007). The variable rotation period of the inner region of Saturn's plasma disk. *Science*, *316*(5823), 442–445. <https://doi.org/10.1126/science.1138562>
- Hansen, C. J., Esposito, L. W., Aye, K.-M., Colwell, J. E., Hendrix, A. R., Portyankina, G., & Shemansky, D. (2017). Investigation of diurnal variability of water vapor in Enceladus' plume by the Cassini ultraviolet imaging spectrograph. *Geophysical Research Letters*, *44*(2), 672–677. <https://doi.org/10.1002/2016GL071853>
- Hashimoto, K., Kudo, S., & Matsumoto, H. (1998b). Source of auroral myriametric radiation observed with Geotail. *Journal of Geophysical Research*, *103*(A10), 23475–23483. <https://doi.org/10.1029/98JA01920>
- Hashimoto, K., Matsumoto, H., Murata, T., Kaiser, M. L., & Bougeret, J.-L. (1998a). Comparison of AKR simultaneously observed by the GEOTAIL and WIND spacecraft. *Geophysical Research Letters*, *25*(6), 853–856. <https://doi.org/10.1029/98GL00385>
- Hess, S., Cecconi, B., & Zarka, P. (2008). Modeling of Io-Jupiter decameter arcs, emission beaming and energy source. *Geophysical Research Letters*, *35*(13), L13107. <https://doi.org/10.1029/2008GL033656>
- Higgins, C. A., Thieman, J. R., Fung, S. F., Green, J. L., & Candey, R. M. (1999). Jovian dual-sinusoidal HOM lane features observed by Galileo. *Geophysical Research Letters*, *26*(3), 389–392. <https://doi.org/10.1029/1998GL900302>
- Holmberg, M. K. G., Wahlund, J.-E., & Morooka, M. W. (2014). Dayside/nightside asymmetry of ion densities and velocities in Saturn's inner magnetosphere. *Geophysical Research Letters*, *41*(11), 3717–3723. <https://doi.org/10.1002/2014GL060229>
- Ingersoll, A. P., & Ewald, S. P. (2017). Decadal timescale variability of the Enceladus plumes inferred from Cassini images. *Icarus*, *282*, 260–275. <https://doi.org/10.1016/j.icarus.2016.09.018>
- Jackman, C. M., Arridge, C. S., Slavin, J. A., Milan, S. E., Lamy, L., Dougherty, M. K., & Coates, A. J. (2010). In situ observations of the effect of a solar wind compression on Saturn's magnetotail. *Journal of Geophysical Research*, *115*(A10), A10240. <https://doi.org/10.1029/2010JA015312>
- Jackman, C. M., Lamy, L., Freeman, M. P., Zarka, P., Cecconi, B., Kurth, W. S., et al. (2009). On the character and distribution of lower-frequency radio emissions at Saturn and their relationship to substorm-like events. *Journal of Geophysical Research*, *114*(A8), A08211. <https://doi.org/10.1029/2008JA013997>
- Jackman, C. M., O'Dwyer, E. P., Louis, C. K., Fogg, A. R., Waters, J. E., & Lamy, L. (2023). Using crossings of Saturn's magnetospheric boundaries to explore the link between upstream conditions and radio emission. In C. K. Louis, C. M. Jackman, G. Fischer, A. H. Sulaiman, P. Zucca, & D. Institute for Advanced Studies (Eds.), *Planetary, solar and heliospheric radio emissions IX*. <https://doi.org/10.25546/103100>
- Kaiser, M. L., Desch, M. D., & Brown, M. E. (1996). Evidence for an Io plasma torus influence on high-latitude Jovian radio emission. *Journal of Geophysical Research*, *101*(A1), 13–18. <https://doi.org/10.1029/95JA02389>
- Kaiser, M. L., Desch, M. D., Warwick, J. W., & Pearce, J. B. (1980). Voyager detection of nonthermal radio emission from Saturn. *Science*, *209*(4462), 1238–1240. <https://doi.org/10.1126/science.209.4462.1238>
- Khurana, K. K., Mitchell, D. G., Arridge, C. S., Dougherty, M. K., Russell, C. T., Paranicas, C., et al. (2009). Sources of rotational signals in Saturn's magnetosphere. *Journal of Geophysical Research*, *114*(A2), A02211. <https://doi.org/10.1029/2008JA013312>
- Kurth, W. S., Gurnett, D. A., Menietti, J., Mutel, R. L., Kivelson, M. G., Bunce, E., et al. (2011). A close encounter with a Saturn Kilometric Radiation source region. In *7th international workshop on planetary, solar and heliospheric radio emissions (PRE VII)* (pp. 75–85). <https://doi.org/10.1553/PRE7s75>
- Ladreiter, H. P., & Leblanc, Y. (1990). Source location of the Jovian hectometric radiation via ray-tracing technique. *Journal of Geophysical Research*, *95*(A5), 6423–6435. <https://doi.org/10.1029/A095iA05p06423>

- Lamy, L. (2017). The Saturnian Kilometric Radiation before the Cassini grand finale. In G. Fischer, G. Mann, M. Panchenko, & P. Zarka (Eds.), *Planetary radio emissions VIII* (pp. 171–190). <https://doi.org/10.1553/PRE8s171>
- Lamy, L., Cecconi, B., Prangé, R., Zarka, P., Nichols, J. D., & Clarke, J. T. (2009). An auroral oval at the footprint of Saturn's Kilometric radio sources, Colocated with the UV Aurorae. *Journal of Geophysical Research*, *114*(A10), A10212. <https://doi.org/10.1029/2009JA014401>
- Lamy, L., Cecconi, B., Zarka, P., Canu, P., Schippers, P., Kurth, W. S., et al. (2011). Emission and propagation of Saturn Kilometric Radiation: Magnetosonic modes, beaming pattern, and polarization state. *Journal of Geophysical Research*, *116*(A4), A04212. <https://doi.org/10.1029/2010JA016195>
- Lamy, L., Prangé, R., Pryor, W., Gustin, J., Badman, S. V., Melin, H., et al. (2013). Multispectral simultaneous diagnosis of Saturn's aurorae throughout a planetary rotation. *Journal of Geophysical Research*, *118*(8), 4817–4843. <https://doi.org/10.1002/jgra.50404>
- Lamy, L., Schippers, P., Zarka, P., Cecconi, B., Arridge, C. S., Dougherty, M. K., et al. (2010). Properties of Saturn Kilometric Radiation measured within its source region. *Geophysical Research Letters*, *37*(12), L12104. <https://doi.org/10.1029/2010GL043415>
- Lamy, L., Zarka, P., Cecconi, B., Hess, S., & Prangé, R. (2008). Modeling of Saturn Kilometric Radiation arcs and equatorial shadow zone. *Journal of Geophysical Research*, *113*(A10), A10213. <https://doi.org/10.1029/2008JA013464>
- Lamy, L., Zarka, P., Cecconi, B., Prangé, R., Kurth, W. S., & Gurnett, D. A. (2008). Saturn Kilometric Radiation: Average and statistical properties. *Journal of Geophysical Research*, *113*(A7), A07201. <https://doi.org/10.1029/2007JA012900>
- Lamy, L., Zarka, P., Cecconi, B., Prangé, R., Kurth, W. S., Hospodarsky, G., et al. (2018). The low-frequency source of Saturn's Kilometric Radiation. *Science*, *362*(6410), eaat2027. <https://doi.org/10.1126/science.aat2027>
- Long, M., Gu, X., Ni, B., Cao, X., Ma, X., & Zhao, Y. (2021). Global distribution of electrostatic electron cyclotron harmonic waves in Saturn's magnetosphere: A survey of over-13-Year Cassini RPWS observations. *Journal of Geophysical Research*, *126*(4), e2020JE006800. <https://doi.org/10.1029/2020JE006800>
- Louarn, P., Kurth, W. S., Gurnett, D. A., Hospodarsky, G. B., Persoon, A. M., Cecconi, B., et al. (2007). Observation of similar radio signatures at Saturn and Jupiter: Implications for the magnetospheric dynamics. *Geophysical Research Letters*, *34*(20), L20113. <https://doi.org/10.1029/2007GL030368>
- Louarn, P., Mauk, B. H., Kivelson, M. G., Kurth, W. S., Roux, A., Zimmer, C., et al. (2001). A multi-instrument study of a Jovian magnetospheric disturbance. *Journal of Geophysical Research*, *106*(A12), 29883–29898. <https://doi.org/10.1029/2001JA900067>
- Louarn, P., Roux, A., Perraut, S., Kurth, W., & Gurnett, D. (1998). A study of the large-scale dynamics of the Jovian magnetosphere using the Galileo plasma wave experiment. *Geophysical Research Letters*, *25*(15), 2905–2908. <https://doi.org/10.1029/98GL01774>
- Louarn, P., Roux, A., Perraut, S., Kurth, W. S., & Gurnett, D. A. (2000). A study of the Jovian “energetic magnetospheric events” observed by Galileo: Role in the radial plasma transport. *Journal of Geophysical Research*, *105*(A6), 13073–13088. <https://doi.org/10.1029/1999JA900478>
- Mutel, R. L., Menietti, J. D., Gurnett, D. A., Kurth, W., Schippers, P., Lynch, C., et al. (2010). CMI growth rates for Saturnian Kilometric radiation. *Geophysical Research Letters*, *37*(19), L19105. <https://doi.org/10.1029/2010GL044940>
- O'Dwyer, E. P., Jackman, C. M., Domijan, K., Lamy, L., & Louis, C. K. (2023). Selection of low frequency extensions of Saturn Kilometric radiation. In C. K. Louis, C. M. Jackman, G. Fischer, A. H. Sulaiman, P. Zucca, & D. Institute for Advanced Studies (Eds.), *Planetary, solar and heliospheric radio emissions IX*. <https://doi.org/10.25546/103103>
- Persoon, A. M., Gurnett, D. A., Kurth, W. S., & Groene, J. B. (2006). A simple scale height model of the electron density in Saturn's plasma disk. *Geophysical Research Letters*, *33*(18), L18106. <https://doi.org/10.1029/2006GL027090>
- Persoon, A. M., Kurth, W. S., Gurnett, D. A., Faden, J. B., Groene, J. B., Morooka, M. W., et al. (2020). Distribution in Saturn's inner magnetosphere from 2.4 to 10 RS: A diffusive equilibrium model. *Journal of Geophysical Research*, *125*(3), 1–15. <https://doi.org/10.1029/2019JA027545>
- Reed, J. J., Jackman, C. M., Lamy, L., Kurth, W. S., & Whiter, D. K. (2018). Low-frequency extensions of the Saturn Kilometric radiation as a proxy for magnetospheric dynamics. *Journal of Geophysical Research*, *123*(1), 443–463. <https://doi.org/10.1002/2017JA024499>
- Schippers, P., Moncuquet, M., Meyer-Vernet, N., & Lecacheux, A. (2013). Core electron temperature and density in the innermost Saturn's magnetosphere from HF power spectra analysis on Cassini. *Journal of Geophysical Research*, *118*(11), 7170–7180. <https://doi.org/10.1002/2013JA019199>
- Sergis, N., Jackman, C. M., Masters, A., Krimigis, S. M., Thomsen, M. F., Hamilton, D. C., et al. (2013). Particle and magnetic field properties of the Saturnian magnetosheath: Presence and upstream escape of hot magnetospheric plasma. *Journal of Geophysical Research: Space Physics*, *118*(4), 1620–1634. <https://doi.org/10.1002/jgra.50164>
- Taubenschuss, U., Lamy, L., Fischer, G., Píša, D., Santolík, O., Souček, J., et al. (2021). The Faraday rotation effect in Saturn Kilometric Radiation observed by the CASSINI spacecraft. *Icarus*, *370*, 114661. <https://doi.org/10.1016/j.icarus.2021.114661>
- Waite, J. H., & Furman, J. D. (2013). *Cassini orbiter SAT/SW CAPS derived electron moments V1.0, CO-S/SW-CAPS-5-DDR-ELE-MOMENTS-V1.0*. NASA Planetary Data System. <https://doi.org/10.17189/1519594>
- Wu, C. S., & Lee, L. C. (1979). A theory of the terrestrial Kilometric radiation. *The Astrophysical Journal*, *230*, 621–626. <https://doi.org/10.1086/157120>
- Wu, S., Taubenschuss, U., Ye, S., Fischer, G., Cecconi, B., Wang, M., et al. (2024). Ray-tracing analysis for the propagation of Saturn narrowband emission within the Saturnian magnetosphere. *Journal of Geophysical Research*, *129*(4), e2023JE008118. <https://doi.org/10.1029/2023JE008118>
- Wu, S. Y., Ye, S., Fischer, G., Wang, J., Long, M., Menietti, J. D., et al. (2021). Statistical study on spatial distribution and polarization of Saturn narrowband emissions. *The Astrophysical Journal*, *918*(2), 64. <https://doi.org/10.3847/1538-4357/ac0af1>
- Wu, S. Y., Ye, S. Y., Fischer, G., Jackman, C. M., Wang, J., Menietti, J. D., et al. (2022b). Reflection and refraction of the L-O mode 5 kHz Saturn narrowband emission by the magnetosheath. *Geophysical Research Letters*, *49*(5), e2021GL096990. <https://doi.org/10.1029/2021GL096990>
- Wu, S. Y., Ye, S. Y., Fischer, G., Taubenschuss, U., Jackman, C. M., O'Dwyer, E., et al. (2022c). Saturn anomalous myriametric radiation, a new type of Saturn radio emission revealed by Cassini. *Geophysical Research Letters*, *49*(16), e2022GL099237. <https://doi.org/10.1029/2022GL099237>
- Wu, S. Y., Zarka, P., Lamy, L., Taubenschuss, U., Cecconi, B., Ye, S. Y., et al. (2022a). Observations of the first harmonic of Saturn Kilometric radiation during Cassini's grand finale. *Journal of Geophysical Research: Space Physics*, *127*(9), 1–12. <https://doi.org/10.1029/2022JA030776>
- Ye, S.-Y., Fischer, G., Menietti, J. D., Wang, Z., Gurnett, D. A., & Kurth, W. S. (2011). An overview of Saturn narrowband radio emissions observed by Cassini RPWS. In H. ~O. Rucker, W. ~S. Kurth, P. Louarn, & G. Fischer (Eds.), *Planetary, solar and heliospheric radio emissions (PRE VII)* (pp. 99–113). <https://doi.org/10.1553/PRE7s99>
- Ye, S.-Y., Gurnett, D. A., Fischer, G., Cecconi, B., Menietti, J. D., Kurth, W. S., et al. (2009). Source locations of narrowband radio emissions detected at Saturn. *Journal of Geophysical Research*, *114*(A6), A06219. <https://doi.org/10.1029/2008JA013855>

- Ye, S.-Y., Menietti, J. D., Fischer, G., Wang, Z., Cecconi, B., Gurnett, D. A., & Kurth, W. S. (2010). Z mode waves as the source of Saturn narrowband radio emissions. *Journal of Geophysical Research*, *115*(A8), A08228. <https://doi.org/10.1029/2009JA015167>
- Young, D. T., Berthelier, J. J., Blanc, M., Burch, J. L., Coates, A. J., Goldstein, R., et al. (2004). Cassini plasma spectrometer investigation. *Space Science Reviews*, *114*(1), 1–112. <https://doi.org/10.1007/s11214-004-1406-4>
- Zarka, P. (1998). Auroral radio emissions at the outer planets: Observations and theories. *Journal of Geophysical Research*, *103*(E9), 20159–20194. <https://doi.org/10.1029/98JE01323>